Macroscopic cross-linked Ni@C composite with high porosity by a novel salt-templating process

Xing Yu, Xuewei Cui, Annie Gagnoud, Yves Fautrelle, René Moreau, Xi Li

Macroscopic cross-linked Ni@C composite with high porosity by a novel salt-templating process

Xing Yu[a], Xuewei Cui[a], Annie Gagnoud[b], Yves Fautrelle[b], René Moreau[b], Xi Li[a,b,*]

[a]State Key Laboratory of Advanced Special Steels, Shanghai University, Shanghai, 200072, PR China
[b]SIMAP-EPM-Madylam/G-INP/CNRS, PHELMA, BP 75, 38402, St Martin d'Heres Cedex, France

A facile and scalable salt-templating strategy is developed for in situ synthesizing 3D porous Ni@C architecture composed of cross-linked belt-like microwires (*b*Ni@C composite). During the process, self-assembled NaCl particles as a structural template were adopted to not only serve as a porogen embedded inside to activate the formation of substantial macropores, mesopores and even micropores with largely increased BET surface area, but also control the morphologies of 3D carbon matrices by tuning the entanglement and cross-linking behaviors of PVA-based complexes. Meanwhile, the Ni nanoparticles are dispersed homogenously inside without aggregation, which have resulted the alteration of magnetic properties in presence of NaCl. The as-obtained ferromagnetic *b*Ni@C composite exhibits a high adsorption capacity for Pb^{2+} with excellent recyclability. The above results suggest an interesting approach for controlling the morphology and properties of 3D carbon matrix by tuning the content of penetrated NaCl particles used for organo-inorganic co-assembly.

1. Introduction

The wastewaters discharged from various industrial activities are causing serious threats to the environment and public health due to the presence of numerous contaminants, especially heavy metal ions [1]. Adsorption treatment for the heavy metal ions, owing to its high efficiency, simplicity of design and ease of operation, seems to be an attractive approach [2]. Magnetic carbon materials have been demonstrated to be efficient absorbents for heavy metal ions, which resulted from their porous structures with large specific surface area and magnetism that can make the absorbents conveniently collected and removed from a large volume of wastewater under a magnetic field [3,4]. As important magnetic material, nickel particles encapsulated in various carbon structures are largely required as absorbents in fields of treatment of heavy metal ions. However, the synthesized nickel nanoparticles were usually coated within a layer of thin carbon shell instead of macroscopic carbon matrix, in a way, which resulted that the specific surface areas increased invisibly and the small nanoparticles generally aggregated together [5–7].

It is believed that the porosity of the carbon matrix is a determined factor affecting the ion-adsorption capacity, and physical template syntheses based on colloidal particles or other sacrifice-templating particles were used to increase the porosity. By coating graphene oxide sheets on the commercial colloidal silica nanoparticles, large mesopores were created to facilitate mass transfer [8,9]. Differing from general 3D mesoporous silica as template, the colloidal silica nanoparticles were added as porogens that inserted into macroscopic carbon matrix [10]. As another additional porogen, $ZnCl_2$ particles were employed to develop pores in the magnetic carbonaceous materials that synthesized via pyrolysis of hydrochar, and the porosity of the samples can be tuned by $ZnCl_2$ content [11–13]. Using a network of nickel as a graphitization catalyst, a substrate and a sacrificial phase, a porous graphite network can be formed by in situ graphitization of amorphous carbon and sintering of the graphite grains [14]. Additionally, a 3D self-assembly of NaCl particles was adopted to serve as a template to direct the growth of 3D porous carbon nanosheet networks anchored by Sn nanoparticles or few-layer MoS_2, and the NaCl particles can be easily removed by water washing [15,16]. Moreover, the low-cost NaCl particles with thermally stable surface

* Corresponding author. SIMAP-EPM-Madylam/G-INP/CNRS, PHELMA, BP 75, 38402, St Martin d'Heres Cedex, France.
E-mail address: lx_net@sina.com (X. Li).

may be suitable as a porogen that penetrated into 3D carbon matrix for promoting the development of pores. Meanwhile, it is noteworthy that to construct porous polymer networks as the precursors of porous carbon materials is a normal-employed method [17]. Polyvinyl alcohol (PVA), a low cost hydrophilic polymer, is frequently used to build 3D matrix for the capabilities to readily cross-link the polymer chains including itself and immobilize metal ions through the considerable amounts of hydroxyl groups [18,19]. Thus, the complexes between PVA and targeted species often lead to the formation of porous materials.

In the present study, we report a novel and scalable in situ synthesis strategy to fabricate 3D porous Ni@C composite consisted of large amounts of belt-like channels cross-linked (designated as *b*Ni@C composite) with a high adsorption capacity of heavy metal ion Pb^{2+}. In this solid-phase synthesis strategy, the cubic NaCl particles, as a special structural template inserted in 3D matrix, can create and enlarge various pores including maropores, mesopores and micropores, and control the morphologies of the macroscopic carbon frameworks by strength the entanglement and cross-linking of PVA-based complexes. The 3D porous carbon material originates from the porous polymer network composed of the building block of metal-PVA complexes as the polymer PVA chains tend to cross-link with other polymer chains via hydrogen bonds for forming the network-like structure. With the help of NaCl particles, the nickel particles encapsulated in the *b*Ni@C composite are homogeneously dispersed with the remarkable increase of BET surface area and alteration of ferromagnetic properties. Meanwhile, the adsorption capacity of heavy ion Pb^{2+} is largely enhanced and can easily separate from the wastewater under the magnetic field.

2. Experimental

2.1. Chemicals

Nickel chloride hexahydrate ($NiCl_2 \cdot 6H_2O$), ferric chloride hexahydrate ($FeCl_3 \cdot 6H_2O$), poly(vinyl alcohol) (PVA), sodium hydroxide (NaOH), sodium chloride (NaCl) and lead nitrate ($Pb(NO_3)_2$) were purchased from Shanghai Chemical Reagents Company. All reagents were used as-received, without further treatment.

2.2. Synthesis of 3D porous Ni@C composites

In a typical synthesis, the metal precursor $NiCl_2 \cdot 6H_2O$ (0.237 g, 1 mmol), 21 mL PVA solution (3 wt%) were dissolved in 30 mL of deionized water, and the pH value was adjusted to 9 with NaOH (1.25 M) solution. After stirring for 30 min, NaCl particles (2 g) were dissolved into the above solution. The resulting mixed solution was dried in a drying oven and obtained a thin sheet. After that, the sheet was calcined at 650 °C for 3 h in a tube furnace under N_2 and then was cooled to room temperature in the presence of N_2. The obtained black product was washed with deionized water several times to dissolve the sodium chloride and then pure 3D porous *b*Ni@C composite was obtained. For comparison, 3D hollow network-like Ni@C framework (*n*Ni@C composite) was also synthesized by carbonizing the mixture of $NiCl_2 \cdot 6H_2O$ and PVA without NaCl at the same conditions as those for the preparation of the *b*Ni@C composite. In addition, the 3D composites synthesized at 550 °C were designated as *n*Ni@C−550 °C (without adding NaCl particles) and *b*Ni@C−550 °C.

2.3. Characterizations

The morphologies and microstructures of as-prepared products were observed by scanning electron microscopy (SEM, Hitachi SU70, 10 kV), transmission electron microscopy (TEM, JEOL JEM-200CX, 160 kV). X-ray diffraction (XRD) measurements were taken on a Rigaku D/max diffractometer with Cu Kα radiation ($\lambda = 0.154178$ nm). The X-ray photoelectron spectrum (XPS) was tested on an ESCAlab 250xi system. Brunauer−Emmett−Teller (BET) surface areas and porosities of the products were determined by nitrogen adsorption and desorption on an Autosorb IQ2 analyzer. The magnetic properties of the samples were investigated using a superconducting quantum interface device (SQUID) magnetometer (Quantum Design PPMS-9). The concentrations of heavy metal ion were determined by inductively coupled plasma atomic emission spectrometry (ICP-AES, Perkin-Elmer, AA800).

2.4. Adsorption isotherm experiments for heavy metal ion Pb^{2+}

At room temperature, 15 mg of macroscopic Ni@C composites including *n*Ni@C and *b*Ni@C composites were introduced to a 40 mL solution of Pb^{2+} with different concentrations. The as-obtained mixed system was dispersed by ultrasonic irradiation for 2 min to ensure sufficient interaction between Ni@C samples and Pb^{2+}. After 3 h to reach complete adsorption equilibrium, the adsorbents were collected under the assistance of magnets, the remaining concentrations of Pb^{2+} were measured via ICP-AES technique.

To test the reusability of the Ni@C composites, the adsorbents were used in five consecutive adsorption/desorption cycles, with 40 mL of 100 mg/L Pb^{2+} solution being used in the adsorption step while 2 M HNO_3 solution in the desorption cycle as desorbing agent.

3. Results and discussion

In the direct synthesis of the macroscopic Ni@C composites, we adopted three strategies. First, the hydrolysis of Ni^{2+} stabilized by PVA was strengthened in presence of NaOH solution and further initiated the entanglement of $Ni(OH)_2$−PVA complexes through intermolecular and intramolecular hydrogen bonds and physical crosslinking [20]. Second, thermally stable salt particles was used as penetrated structure-template for fabricating porous structures and morphology control. Third, $Ni(OH)_2$−PVA complex was used as the precursor of both nickel and carbon. As illustrated in Fig. 1, For the fabrication process of the porous network-like Ni@C composite (designated as *n*Ni@C composite) without adding NaCl particles, the aqueous solutions of $NiCl_2 \cdot 6H_2O$ and PVA were mixed together, and the resulting Ni^{2+}−PVA complexes converted into $Ni(OH)_2$−PVA complexes and entangled with each other with addition of NaOH solution. Subsequently, the mixed solution was dried at 80 °C. During the process, the ambient pressure helped to maintain a large amount of maropores derived from the entanglement of $Ni(OH)_2$−PVA complexes and a 3D porous network of $Ni(OH)_2$−PVA complexes developed with the presence of a few self-synthesized NaCl particles (Fig. 2a and b). Upon heating under N_2 atmosphere, the Ni@C composite was formed from the precursor $Ni(OH)_2$−PVA complexes and kept the macroscopic porous network (Fig. 2d). However, after adding extra NaCl particles, the $Ni(OH)_2$−PVA complexes entangled much more dramatically and a thin sheet with pale green was obtained after drying (Fig. 2c). The corresponding calcined hollow 3D Ni@C framework composed of 1D cross-linking belt-like microwires created (designated as *b*Ni@C composite) (Fig. 2e). It should be noted the NaCl particles as a porogen embedded into the 3D architecture can tune the entanglement behavior of the $Ni(OH)_2$−PVA complex and excavate pores like mice.

A series of X-ray diffraction (XRD) experiments were performed to reveal the crystallographic structures of the macroscopic Ni@C composites prepared at different conditions. As shown in Fig. 3, for *n*Ni@C−550 °C composite after calcining without final washing,

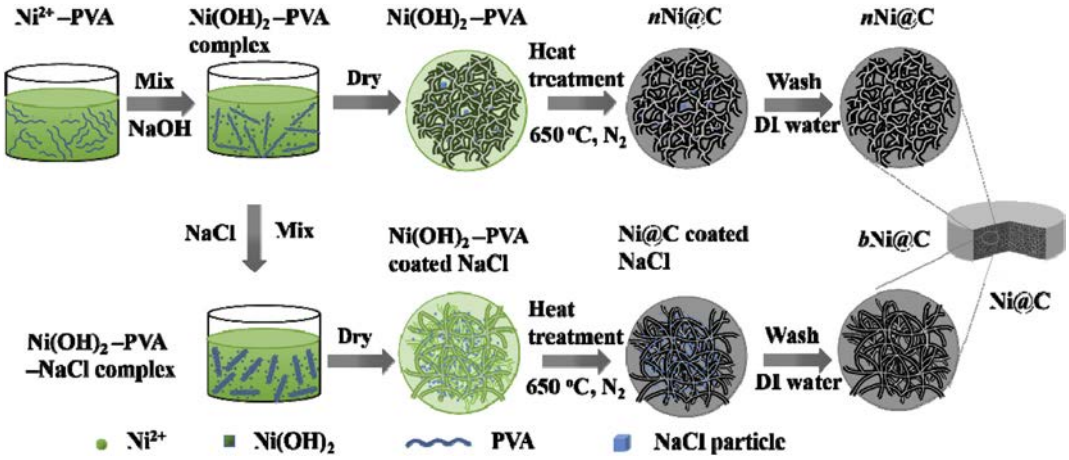

Fig. 1. Schematic illustration of the formation mechanism of the 3D Ni@C composites.

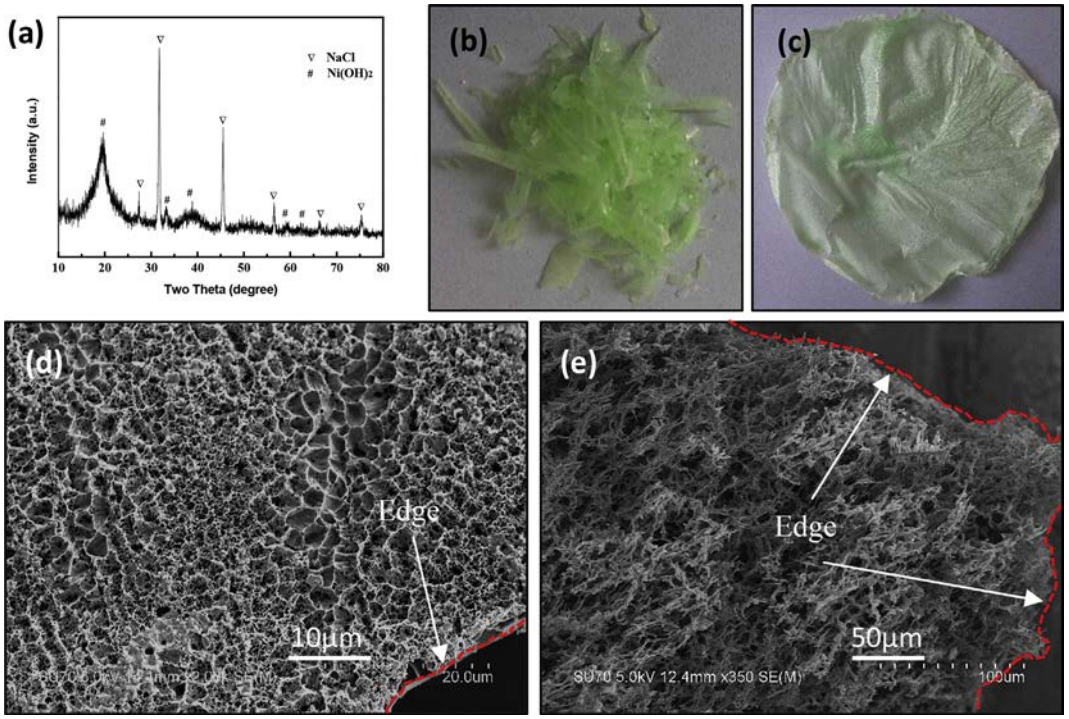

Fig. 2. (a) XRD pattern of the precursor showed in (b), indicating the presence of medium product of $Ni(OH)_2$ with self-synthesized NaCl. The precursors of (b) *n*Ni@C and (c) *b*Ni@C composites after drying, respectively. Low-magnification SEM images of the 3D macroscopic (d) *n*Ni@C and (e) *b*Ni@C composites.

several diffraction peaks corresponding to the cubic phase NaCl (JCPDS card no. 88-2300) are observed from the XRD pattern, indicating that there are a few NaCl particles synthesized during the drying process even though the sample was prepared in absence of NaCl. Here, an idea seeds out that adding substantial extra NaCl particles may be conducive to the presence of porous carbon matrix. From bottom to up, three characteristic peaks marked with (111), (200), (220) planes of the face-centered cubic (fcc) nickel (JCPDS card no. 04-0850) are all presented in the four XRD patterns. However, with the elevation of temperature, the diffraction peaks become higher and narrower, implying that the crystallinity of the products is continuously improved, and it is noteworthy that the carbon converted from amorphous structure (550 °C) to well-developed graphitic structure with the interplanar distance d_{002} of about 0.342 nm (650 °C) are also detected from (002) peaks at around 25° [21,22]. For a comparison, the peak intensities of the *n*Ni@C composite are slight stronger than that of the *b*Ni@C composite, resulting from the liner aggregation (as can be seen later) prepared in absence of NaCl. However, the peak sharpness is reverse, which can be confirmed with the average particle sizes of Ni nanoparticles calculated from the largest diffraction peak (111) by using Scherer's formula, and the estimated average particle sizes are 34.4 nm and 38.9 nm, respectively.

The morphologies and microstructures of as-prepared two distinctly different 3D Ni@C composites were characterized by SEM. For the *n*Ni@C composite synthesized without adding NaCl particles, a 3D hollow network microstructure with well-developed open pores (Fig. 4a and b) appears, and the formation of dense

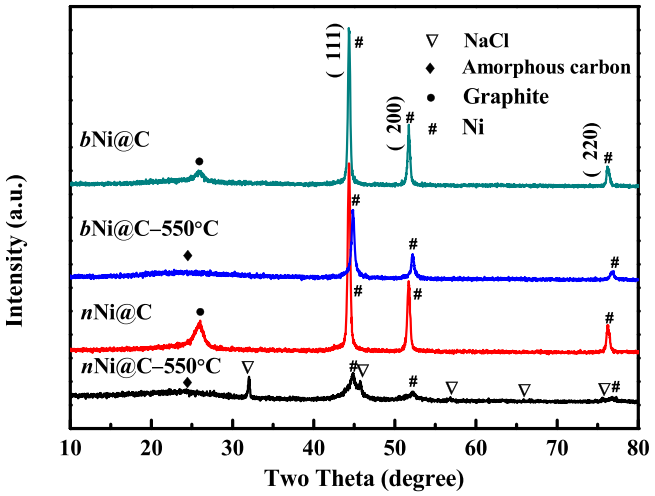

Fig. 3. XRD patterns of the 3D Ni@C composites synthesized at different conditions.

small pores resulted from the collapse of honeycomb-like structure with pseudohexagonal channels. If the amount of precursor $NiCl_2 \cdot 6H_2O$ was reduced to 0.4 mmol or 0.7 mmol (Fig. S1a and b), the as-obtained products showed incompletely hollow structures with various blocked surface areas, and demonstrated that the increasing amounts of $NiCl_2 \cdot 6H_2O$ attributed to the formation of hollow porous structure. These results originated from much more and stronger complexation of $Ni(OH)_2$—PVA with higher ration of metal precursor to carbon precursor, leading to the entanglement of $Ni(OH)_2$—PVA complexes with the help of PVA cross-linking [20]. As a result of addition of 2 g NaCl, the SEM image in Fig. 4c shows a particular structure composed of cross-linked belt-like microwires with large number of swelling joints. The microwires with a rough surface like the skin of toad (Fig. 4d) contain all Ni nanoparticles encapsulated inside, and this core-shell structure can be confirmed by surface-sensitive XPS spectrum (Fig. 4e) that there are two quite week signals of Ni 2p1/2 and 2p3/2 at about 870.2 and 852.8 eV, respectively [23]. Furthermore, the introduction of NaCl particles has resulted the dramatic increases in the size and wall (channels or microwires) thickness of the macropores in the *b*Ni@C composite in comparison with that of *n*Ni@C composite. Meanwhile, the marcopores seem to be stretched along one direction as the white arrow marked in Fig. 4c. These interesting conversions arise from the addition of NaCl particles as a structural template (Fig. 4f). Detailed, the NaCl particles, in a way, strength the interactions including

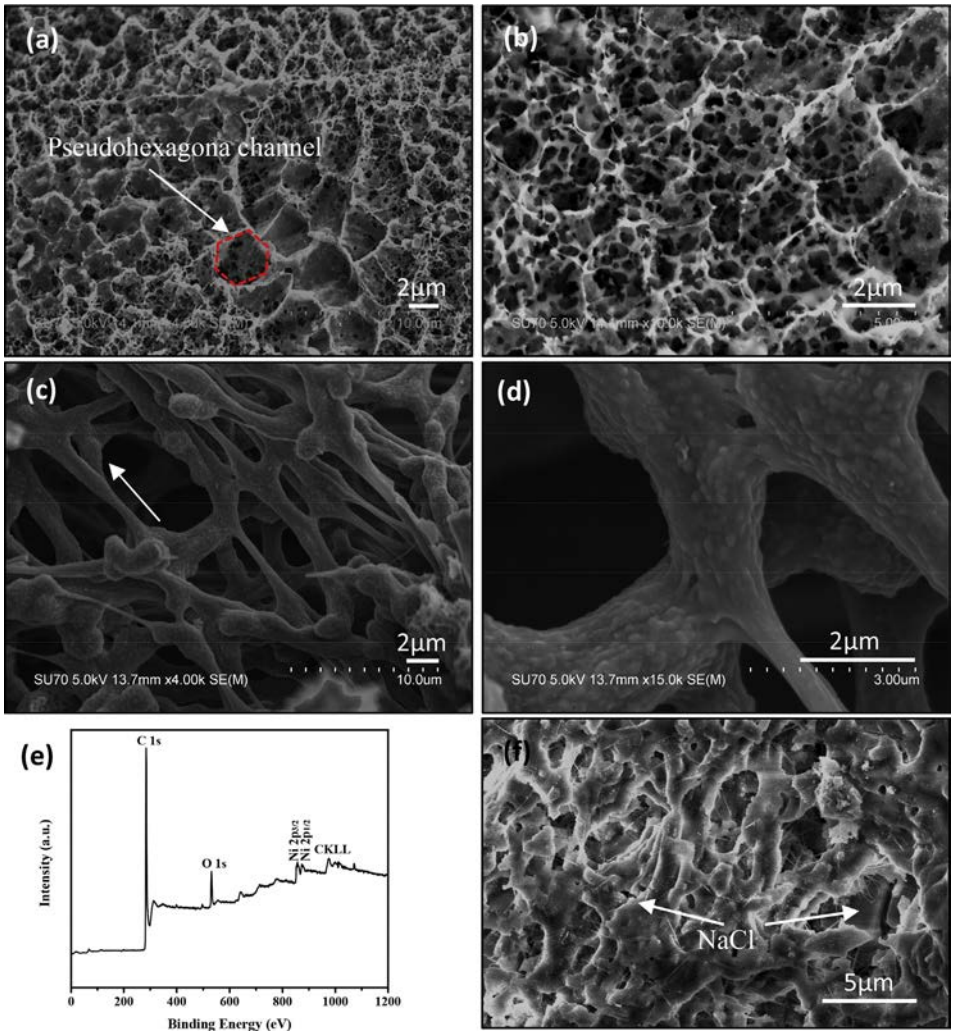

Fig. 4. SEM images with different magnifications of 3D (a, b) network *n*Ni@C composites and (c, d) *b*Ni@C composites prepared using 1 mmol $NiCl_2 \cdot 6H_2O$. (e) XPS spectrum of the *b*Ni@C composites. (f) SEM image of the belt-like Ni@C microwires coated on NaCl template.

physical cross-linking among the $Ni(OH)_2$—PVA complexes through intermolecular and intramolecular hydrogen bonds. Consequently, the close entanglement of $Ni(OH)_2$—PVA complexes are increased dramatically, resulting the formation of large-size belt-like microwires with Ni nanoparticles wrapped inside. The SEM images of products in Fig. S1 indicated that the morphologies of *n*Ni@C composites can be controlled by tuning the adding amount of NaCl particles. On another hand, the NaCl particles, as a special porogen, further create and enlarge the pores after washing. This porous structure would exhibit excellent mass transfer performance, producing good adsorption capacity for heavy metal ions [24].

On the basis of the results shown above, TEM were conducted to investigate the detailed distribution of Ni nanoparticles in these carbon matrix. The TEM analyses of *n*Ni@C composite reveal (Fig. 5a and b) that the Ni nanoparticles are agglomerated into one-dimensional nanochains encapsulated within carbon films, and the nanochains as the channels are cross-linked into 3D network. This result exactly confirms that the $Ni(OH)_2$—PVA complexes have entangled and cross-linked with each other for the formation of the channels of Ni@C network. Except the Ni nanoparticles in the nanochains, the others are dispersed relatively uniformly just like plums in pudding and the average size is about 35 nm in agreement with that XRD indicates. In relative to *n*Ni@C composite, we observe that the Ni nanoparticles in the *b*Ni@C composite are homogeneously dispersed in the carbon films without obvious aggregation (Fig. 5c). Meanwhile, these Ni nanoparticles with an average size of 40 nm nucleated and grew accompanying with substantial voids (Fig. 5d). Combined with the analysis of SEM images, the addition of a mass of NaCl particles promotes the entangling of the $Ni(OH)_2$—PVA complexes into the belt-like microwires, and the fine carbon nanostructure of the composite (Fig. S2) exhibits a porous nanostructure with a few residual nanoparticles studded around PVA-derived dense silk-like filaments, also indicating the intense entanglement of $Ni(OH)_2$—PVA complexes. However, the Ni nanoparticles aren't aggregated as those in the *n*Ni@C composite due to the hindering of the penetrated NaCl particles in the microwires as confirmed by the voids inside. The above results have demonstrated that the presence of NaCl particles can also create numerous mesopores and even micropores to facilitate the heavy metal ions penetration and diffusion. Furthermore, the disappearance of 1D nanochain aggregation of Ni nanoparticles with high shape anisotropy and uniformly dispersed Ni nanoparticles arising caused by the introduction of NaCl particles within the *b*Ni@C composite have resulted the dramatically decrease of saturation magnetization and coercivity (Fig. 6a and Table 1) [25]. However, the two samples show ferromagnetic properties revealed by the inset image in Fig. 6a that the *b*Ni@C composite was attracted to the magnet, which endows them to be magnetically separable adsorbents for heavy metal ions. More importantly, our results suggest an interesting approach for controlling the morphology of 3D carbon matrix and inserted nanocrystals by tuning the content of penetrated NaCl particles used for organo-inorganic co-assembly.

Nitrogen adsorption—desorption measurements are carried out at 77 K to further study the textural characteristics of the Ni@C composites. As shown in Fig. 6b, the isotherm profiles of the *n*Ni@C and *b*Ni@C composites are quite similar and can be categorized as type IV with large hysteresis loops observed at a relative pressure of $p/p0 \approx 0.45$—0.97, implying the existence of a large number of micropores and mesopores in the frameworks of the two Ni@C composites. The pore structures can be further verified by pore sizes distributions based on density functional theory (DFT) in Fig. 6c. Broad pore size distributions in the range less than 33.2 nm for both Ni@C composites can be seen, and show the consistent preponderances of 4 nm mesopores. However, the total pore volume of the *b*Ni@C composite (about 0.227 cm^3/g) increases dramatically from that of the *n*Ni@C composite (about 0.136 cm^3/g) after adding NaCl particles. In addition, the BET specific surface area of the *n*Ni@C composite is measured to be 177.8 m^2/g, which is

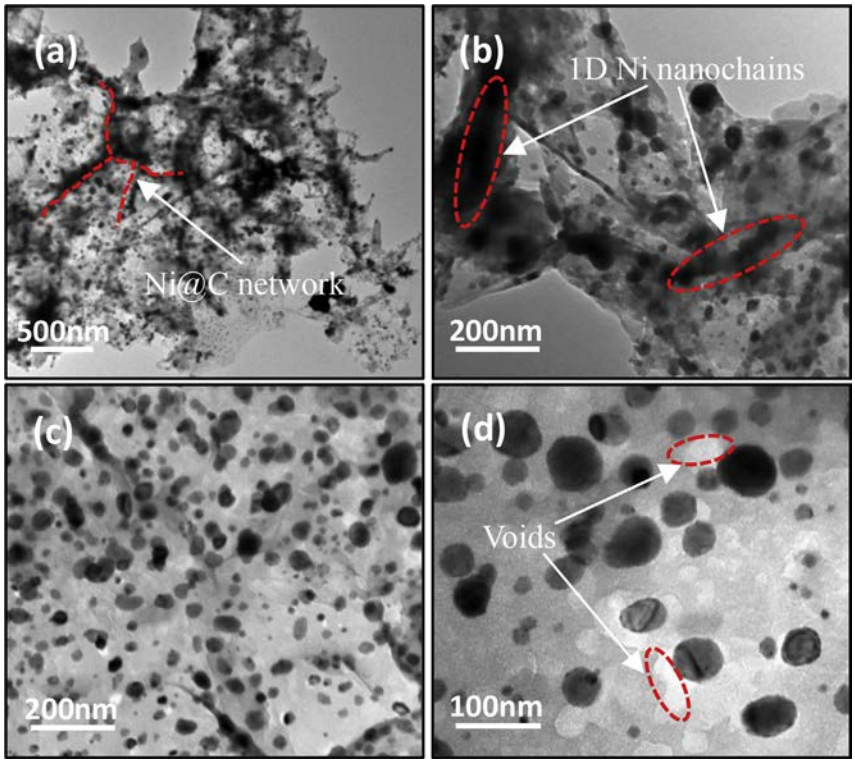

Fig. 5. TEM images with various magnifications of (a, b) *n*Ni@C composites and (c, d) *b*Ni@C composites.

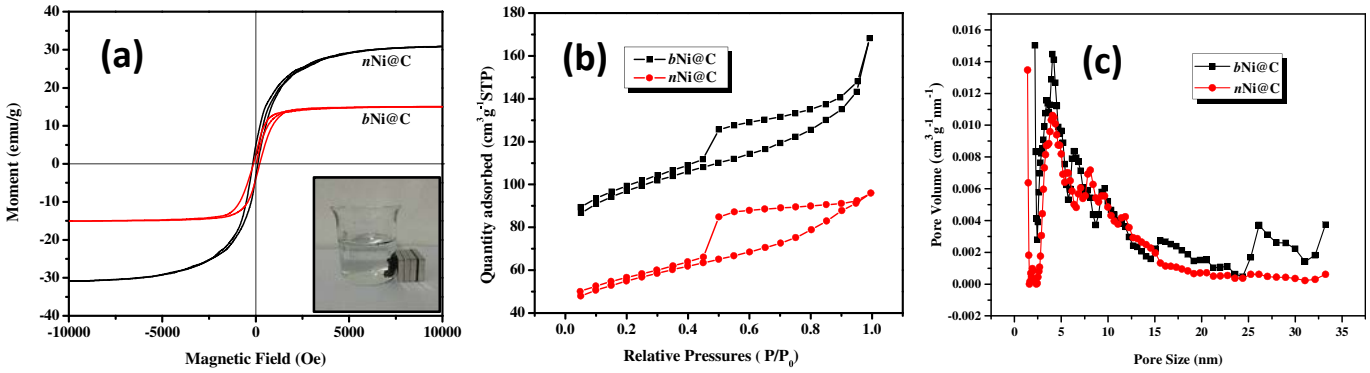

Fig. 6. (a) Room-temperature M–H hysteresis curves of the Ni@C composites. Inset: Photograph (lower right) of the magnetic property of the *b*Ni@C composites under a magnet. (b) N_2 adsorption–desorption isotherms and (c) corresponding pore size distribution curves of the Ni@C composites.

Table 1
Magnetic properties of the Ni@C samples.

Samples	M_s (emu g^{-1})	M_r (emu g^{-1})	H_c (Oe)
*b*Ni@C	15	3.1	94.9
*n*Ni@C	30.8	5.4	152.9

much lower than that of the *b*Ni@C composite (about 307.6 m^2/g). The above evidence demonstrates that the total pore volume and BET specific surface area can be improved greatly in presence of NaCl particles. The larger surface area and well developed 3D porous structures of macropores, mesopores and micropores may be very favorable to the heavy metal ions diffusion to active sites with less resistance during the ions insertion.

To gain insight of effect of the addition of NaCl particles on the adsorption capacity for heavy ions, the Pb^{2+} as a primarily highly toxic pollutant was used as an evidence for the *n*Ni@C and *b*Ni@C composites. Fig. 7a shows the adsorption rate to test the adsorption kinetics of our absorbents at room temperature. When the initial concentration of Pb^{2+} was 100 mg/L, about 78% of the heavy ion for the *b*Ni@C composite was absorbed from the water within 20 min, while only 54% absorption appeared employing the *n*Ni@C composite as the absorbent. The adsorption behaviors of the two absorbents for Pb^{2+} were depicted by adsorption isotherms in Fig. 7b, which well fitted with the Langmuir isotherm model [26]. The calculated maximum adsorption for the *b*Ni@C composite was 178.7 mg/g, which was superior to the *n*Ni@C composite (124.2 mg/g), and much higher than those from previously reported Ni@C nanocomposites [5,6]. The heavy ion was adsorbed on the surface of the macroporous materials through van der Waals force and static electric attraction [27]. The porous structure with high special surface area and surface defects, which provide high available surface adsorption site density and more adsorption sites, is an important factor affecting the ion-adsorption capacity of the composites. As discussed earlier, the NaCl particles, as a structural template, provide much more macropores, mesopores and micropores and higher special surface areas as well as surface defects. Thus the *b*Ni@C composite exhibited much more excellent adsorption behavior than the *n*Ni@C composite. However, the recovery efficiencies of Pb^{2+} on the two Ni@C composites (Fig. 7c) were almost identical that >90% of the total adsorbed Pb^{2+} can be recovered after five recycling tests, which can be attributed to the simple physical adsorption without chemical interaction. Based on the above results, the addition of NaCl particles can enhanced the adsorption capacity of heavy ions by greatly increasing the BET surface areas of the *b*Ni@C composite.

We found this novel fabrication process employing NaCl particles as the structural template to be a general approach for controlling the morphology of carbon matrix. By controlling the PH values and the calcination temperatures, we produced the macroscopic porous Fe@C and $FeNi_3$@C composites with network morphology (Figs. 8 and 9). Upon adding NaCl particles, 3D hollow belt-like cross-linked frameworks resulted and the belt-like microwires also contained a large amount of pores. These results confirm that NaCl particles penetrated within the macroscopic matrix can be used a novel structure-controller by tuning the organo-inorganic complex co-assembly for the growth of 3D carbon-based composites.

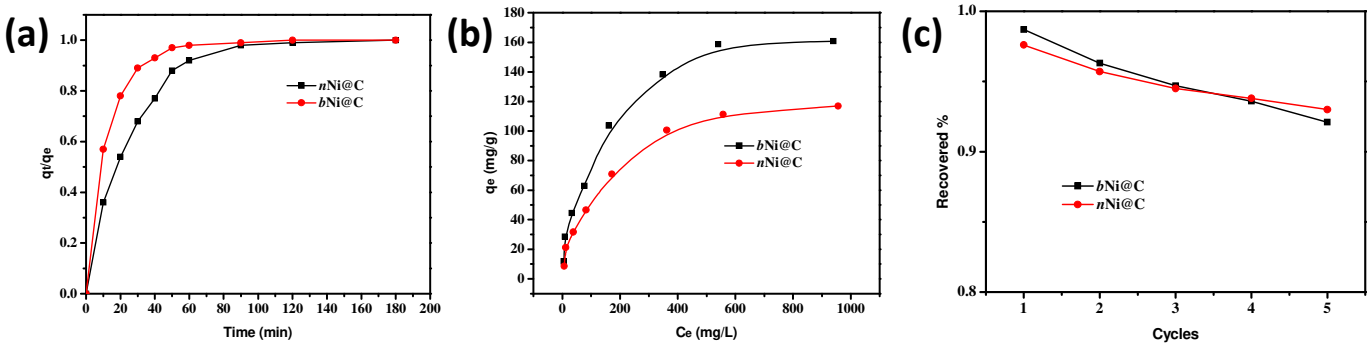

Fig. 7. (a) Time-dependent adsorption capacity of Pb^{2+} with the initial concentration of 100 mg L^{-1}, (b) adsorption isotherms of Pb^{2+} and (c) the recycling tests for adsorption of Pb^{2+} on the *n*Ni@C and *b*Ni@C composites. q_t and q_e is the adsorption capacity at time *t* and equilibrium capacity (mg L^{-1}), respectively. C_e is the equilibrium solute concentration (mg L^{-1}).

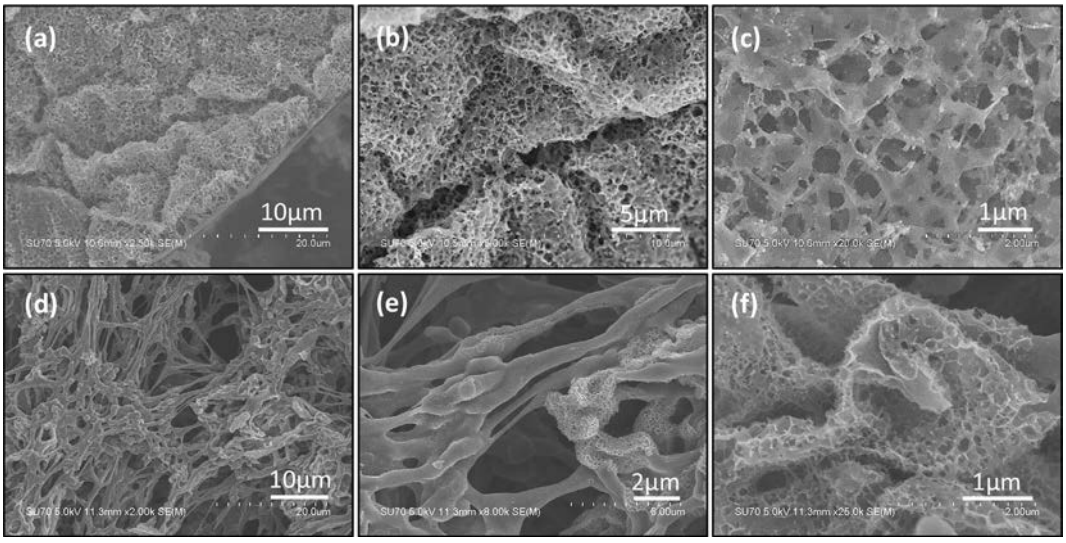

Fig. 8. SEM images with various magnifications of (a–c) 3D network-like Fe@C composites synthesized without addition of NaCl particles and (d–f) 3D cross-linked belt-like Fe@C composites synthesized with addition of NaCl particles.

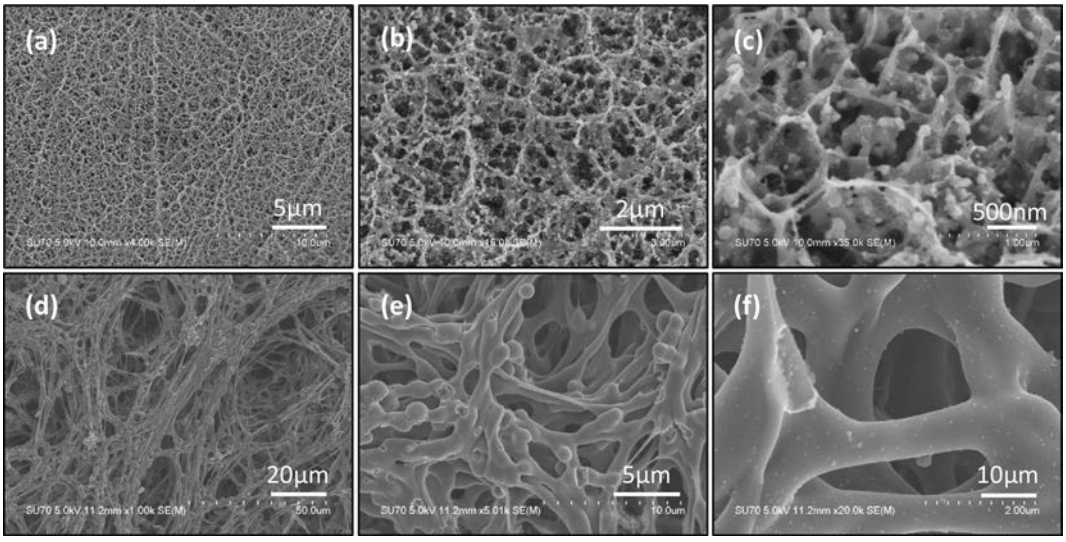

Fig. 9. SEM images with various magnifications of (a–c) 3D network-like $FeNi_3$@C composites synthesized without addition of NaCl particles and (d–f) 3D cross-linked belt-like $FeNi_3$@C composites synthesized with addition of NaCl particles.

4. Conclusions

In summary, NaCl particles, as a structural template, were employed in the process of pyrolysis of porous metal-PVA network for the macroscopic Ni@C composites. In this salt-templating synthesis strategy, the morphologies of the 3D carbon framework and the penetrated Ni nanoparticles are effectively tuned by the contents of NaCl particles. Moreover, the porosity and magnetic properties are remarkably altered in presence of salt particles. The above transformations, in a word, are beneficial to the adsorption capacity for heavy metal ion Pb^{2+} and the *b*Ni@C composites exhibited enhanced adsorption capacity in comparison with *n*Ni@C composites. In addition, this interesting approach can be appropriately applied in the synthesis of other metal@carbon composites, such as 3D Fe@C and $FeNi_3$@C composites.

Acknowledgment

This work is supported partly by the European Space Agency through the Bl-inter 09_473220, National Natural Science Foundation of China (Nos. 51271109 and 51571137) and the Program for Professor of Special Appointment (Eastern Scholar) at Shanghai Institutions of Higher Learning.

Appendix A. Supplementary data

Supplementary data related to this article can be found at http://dx.doi.org/10.1016/j.jallcom.2016.06.248.

References

[1] J.O. Nriagu, J.M. Pacyna, Quantitative assessment of worldwide contamination of air, water and soils by trace metals, Nature 333 (1988) 134–139.
[2] C.Y. Cao, J. Qu, W.S. Yan, J.F. Zhu, Z.Y. Wu, W.G. Song, Low-cost synthesis of

flowerlike α-Fe_2O_3 nanostructures for heavy metal ion removal: adsorption property and mechanism, Langmuir 28 (2012) 4573−4579.
[3] W.J. Zhang, X.H. Shi, Y.X. Zhang, W. Gu, B.Y. Li, Y.Z. Xian, Synthesis of water-soluble magnetic graphene nanocomposites for recyclable removal of heavy metal Ions, J. Mater. Chem. A 1 (2013) 1745−1753.
[4] L.L. Fan, C.N. Luo, M. Sun, X.J. Li, H.M. Qiu, Highly selective adsorption of lead ions by water-dispersible magnetic chitosan/graphene oxide composites, Colloid Surf. B 103 (2013) 523−529.
[5] Y.H. Ni, L. Jin, L. Zhang, J.M. Hong, Honeycomb-like Ni@C composite nanostructures: synthesis, properties and applications in the detection of glucose and the removal of heavy-metal ions, J. Mater. Chem. 20 (2010) 6430−6436.
[6] Z.H. Xiao, R. Zhang, X.Y. Chen, X.L. Li, T.F. Zhou, Magnetically recoverable Ni@carbon nanocomposites: solid-state synthesis and the application as excellent adsorbents for heavy metal ions, Appl. Surf. Sci. 263 (2012) 795−803.
[7] L. Ning, X.G. Li, Y.L. Sun, X.H. Wang, Synthesis and characteristic of carbon encapsulated ferronickel nanoparticles by detonation decomposition of doping with nitrate explosive precursors, J. Alloys Compd. 505 (2010) 352−356.
[8] J. Liang, Y. Jiao, M. Jaroniec, S.Z. Qiao, Sulfur and nitrogen dual-doped mesoporous graphene electrocatalyst for oxygen reduction with synergistically enhanced performance, Angew. Chem. Int. Ed. 51 (2012) 11496−11500.
[9] W. Wei, H.W. Liang, K. Parvez, X.D. Zhuang, X.L. Feng, K. Müllen, Nitrogen-doped carbon nanosheets with size-defined mesopores as highly efficient metal-free catalyst for the oxygen reduction reaction, Angew. Chem. Int. Ed. 126 (2014) 1596−1600.
[10] H.W. Liang, W. Wei, Z.S. Wu, X.L. Feng, K. Mullen, Mesoporous metal−nitrogen-doped carbon electrocatalysts for highly efficient oxygen reduction reaction, J. Am. Chem. Soc. 135 (2013) 16002−16005.
[11] X. Zhu, Y. Liu, G. Luo, F. Qian, S. Zhang, J. Chen, Facile fabrication of magnetic carbon composites from hydrochar via simultaneous activation and magnetization for triclosan adsorption, Environ. Sci. Technol. 48 (2014) 5840−5848.
[12] C. Falco, J.P. Marco-Lozar, D. Salinas-Torres, E. Morallón, D. Cazorla-Amorós, M.M. Titirici, et al., Tailoring the porosity of chemically activated hydrothermal carbons: influence of the precursor and hydrothermal carbonization temperature, Carbon 62 (2013) 346−355.
[13] X. Zhu, F. Qian, Y. Liu, S. Zhang, J.M. Chen, Environmental performances of hydrochar-derived magnetic carbon composite affected by its carbonaceous precursor, RSC Adv. 5 (2015) 60713−60722.
[14] B.B. Bokhonov, D.V. Dudina, A.V. Ukhina, M.A. Korchagin, N.V. Bulina, V.I. Mali, A.G. Anisimov, Formation of self-supporting porous graphite structures by Spark Plasma Sintering of nickel-amorphous carbon mixtures, J. Phys. Chem. Solids 76 (2015) 192−202.
[15] J. Qin, C. He, N. Zhao, Z. Wang, C. Shi, E.Z. Liu, J. Li, Graphene networks anchored with Sn@graphene as lithium ion battery anode, ACS Nano 8 (2014) 1728−1738.
[16] J.W. Zhou, J. Qin, X. Zhang, C.S. Shi, E.Z. Liu, J.J. Li, N.Q. Zhao, C.N. He, 2D space-confined synthesis of few-layer MoS_2 anchored on carbon nanosheet for lithium-ion battery anode, ACS Nano 9 (2015) 3837−3848.
[17] B. Liu, H. Shioyama, T. Akita, Q. Xu, Metal−organic framework as a template for porous carbon synthesis, J. Am. Chem. Soc. 130 (2008) 5390−5391.
[18] G.L. Du, L. Nie, G.R. Gao, Y.N. Sun, R.X. Hou, H. Zhang, T. Chen, J. Fu, Tough and biocompatible hydrogels based on in situ interpenetrating networks of dithiol-connected graphene oxide and poly(vinyl alcohol), ACS Appl. Mater. Interfaces 7 (2015) 3003−3008.
[19] S.A. Poursamar, M. Azami, M. Mozafari, Controllable synthesis and characterization of porous polyvinyl alcohol/hydroxyapatite nanocomposite scaffolds via an in situ colloidal technique, Colloids Surf. B Biointerfaces 84 (2011) 310−316.
[20] X. Li, Y. Li, S. Zhang, Z. Ye, Preparation and characterization of new foam adsorbents of poly(vinyl alcohol)/chitosan composites and their removal for dye and heavy metal from aqueous solution, Chem. Eng. J. 183 (2012) 88−97.
[21] Z.C. Yang, J.G. Shen, L.A. Archer, An in situ method of creating metal oxide−carbon composites and their application as anode materials for lithium-ion batteries, J. Mater. Chem. 21 (2011) 11092−11097.
[22] E. Kang, Y.S. Jung, A.S. Cavanagh, G.H. Kim, S.M. George, A.C. Dillon, et al., Fe_3O_4 nanoparticles confined in mesocellular carbon foam for high performance anode materials for lithium-ion batteries, Adv. Funct. Mater 21 (2011) 2430−2438.
[23] W.F. Chen, S.R. Li, C.H. Chen, L.F. Yan, Self-assembly and embedding of nanoparticles by in situ reduced graphene for preparation of a 3D graphene/nanoparticle aerogel, Adv. Mater. 23 (2011) 5679−5683.
[24] H. Li, J.C. Fan, Z.X. Shi, M. Lian, M. Tian, J. Yin, Preparation and characterization of sulfonated graphene-enhanced poly (vinyl alcohol) composite hydrogel and its application as dye absorbent, Polymer 60 (2015) 96−106.
[25] X. Ni, Q. Zhao, D. Zhang, X. Zhang, H. Zheng, Novel hierarchical nanostructures of nickel: self-assembly of hexagonal nanoplatelets, J. Phys. Chem. C 111 (2007) 601−605.
[26] I. Langmuir, The adsorption of gases on plane surfaces of glass, mica and platinum, J. Am. Chem. Soc. 40 (1918) 1361−1403.
[27] Y.X. Song, T.T. Qiang, M. Ye, Q.Y. Ma, Z. Fang, Metal organic framework derived magnetically separable 3-dimensional hierarchical Ni@C nanocomposites: synthesis and adsorption properties, Appl. Surf. Sci. 359 (2015) 834−840.